ESTIMATION OF COMPOSITE THERMAL CONDUCTIVITY OF A HETROGENEOUS METHANE HYDRATE SAMPLE USING iTOUGH2

Arvind Gupta[1], Timothy J. Kneafsey[2], George J. Moridis[2], Yongkoo Seol[2],
Michael B. Kowalsky[2], E. D. Sloan, Jr.[1]

(1) Center for Research on Hydrates, Colorado School of Mines, Golden, CO-80401, USA
(2) Earth Sciences Divison, Lawrence Berkeley National Laboratory, Berkeley, CA-94720, USA

e-mail: argupta@mines.edu

ABSTRACT

We determined the composite thermal conductivity (k_θ) of a porous methane hydrate sample (composed of hydrate, water, and methane gas) as a function of density using iTOUGH2. X-ray computed tomography (CT) was used to visualize and quantify the density changes that occurred during hydrate formation from granular ice. The composite thermal conductivity was estimated and validated by minimizing the differences between the observed and the predicted thermal response using history matching. The estimated density-dependent composite thermal conductivity ranged between 0.25 and 0.58 W/m/K.

NOMENCLATURE

C	specific heat (J/kg/K)
k	thermal conductivity (W/m/K)
S	phase saturation
φ	porosity
V	volume (m^3)
m	mass (kg)
ρ	density (kg/m^3)
X	mass fraction
r	radius

SUBSCRIPTS AND SUPERSCRIPTS

H	Hydrate
I	Ice
G	Gas
W	Water
z	Zone

INTRODUCTION

Natural gas clathrate hydrates are a class of inclusion compounds that are formed from a network of water molecules that encapsulate small gas molecules [*Sloan*, 1998]. In general, hydrates form at high pressures and low temperatures in the presence of water and the hydrate's former gas (i.e., methane, ethane). Gas hydrate deposits are estimated to contain significant amounts of hydrocarbons (mainly methane) on the order of $1–5\times10^{15}$ m^3 at STP [*Milkov*, 2004] . Therefore, these deposits present a potentially important future energy resource. Recovery of even a fraction of the estimated hydrocarbons contained within the hydrates would provide a substantial alternative resource of energy.

Hydrate thermal properties play an important role in assessing gas production from natural deposits, seafloor stability of hydrate-bearing oceanic sediments, global climate change, submarine slide formation, and hydrate plug dissociation in oil and gas pipelines [*Peters et al.*, 2000; *Ruppel*, 2000]. Thus, thermal property measurements are crucial in quantifying the role of gas hydrates in these applications. Despite the importance of hydrate thermal properties, few measurements of the methane hydrate thermal conductivity are available in the literature.

We used X-ray CT to visualize and quantify the physical state of the sample (i.e., the distribution of the unreacted water and the density changes that occurred during the hydrate formation process). This paper presents a new technique to estimate the k_θ of porous hydrate samples, and demonstrates the application of inverse-modeling using iTOUGH2 in hydrate physical and thermal property measurements.

EXPERIMENTAL METHOD

The experiment was performed in a 7.6 cm i.d. × 26.7 cm long cylindrical aluminum vessel that is transparent to X-rays. The same experimental set-up was used to study the hydrate formation and dissociation processes in sediments [*Kneafsey et al.*, 2005]. A temperature controller was used to maintain the coolant temperature to within ± 0.2 K. Pressure

was measured within ±0.007 MPa on the gas inlet line using a Rosemount 1151 pressure transducer. Three type-T thermocouples (18 inches long, 1/16 inch diameter, Omega Engineering, Stamford CT) were used to measure the hydrate sample thermal response. A fourth thermocouple was placed in the vertical direction aligned with the vessel center. For modeling purposes, the exact position of each thermocouple with respect to the vessel center was determined from the CT images.

In this work, we used a modified Siemens Somatom HiQ medical CT scanner with an x-ray energy of 133 keV and a current of 120 mA to collect the hydrate sample images. The CT images provide a measure of material density within a specific volume of 250 μm x 250 μm × 5mm (voxel). In our study, axial cross sections of 5 mm thick slices were obtained along the entire sample length, for a total of 54 images.

HYDRATE FORMATION

Methane hydrate was formed in the vessel from 250–850 μm size granular ice particles (*Stern et al.*, 1996). The initial porosity of the sample (defined as the volume ratio of pore space filled with gas to the total vessel volume) was estimated to be 32%. After packing with ice, the pressure vessel was transferred to the CT table, and the fluid jacket was connected to the coolant line carrying fluid at 265K.

Methane hydrate was formed by slowly pressurizing the vessel to 6.2 MPa with 99.9% pure methane gas at 265 K. Figure 1 shows the decrease in pressure with time as methane gas was consumed during the conversion of ice into methane hydrate. Figure 1 also shows the temperature profiles at the measured locations during hydrate formation in the closed system. The bath temperature was raised step-wise to the ice point to enhance the hydrate formation by melting the ice. Based on gas consumption and assuming a hydration number equal to 6.0, 91 ± 2 % (by mass) of ice was converted into hydrate over 2 days. The final product was thus a porous heterogeneous sample comprised of a matrix of solid methane hydrate, with pores filled with water and methane gas.

DETERMINATION OF SAMPLE COMPOSITE DENSITY AND SPECIFIC HEAT

Figure 2 shows the axially averaged sample CT images before and after hydrate formation. Thus, Figure 2a shows granular ice and methane gas, and Figure 2b shows methane hydrate, free methane gas, and water. We employed the image processing program ImageJ [*Abramoff et al.*, 2004] to convert x-ray attenuation distributions to composite density (ρ_θ), using a calibration curve determined from x-ray attenuation and material density.
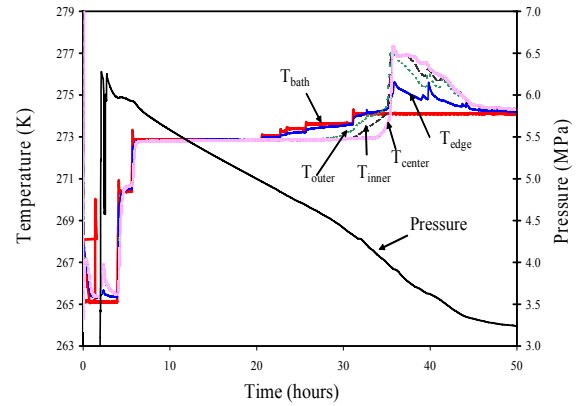

Figure 1.   Pressure and temperatures during hydrate formation.

Figure 3 shows the variation of composite density, ρ_θ in the radial direction before and after hydrate formation. The composite density of porous ice was determined from the CT images (averaging the density along the entire radial direction from 0 to 3.8 cm at t=0 hours) to be about 643 kg/m^3, which is within 1% of the composite density determined according to:

$$\rho_\theta = \rho_I \left(1 - \varphi \right) + \rho_G \varphi \qquad (1)$$

The composite density of 635 kg/m^3 was calculated based on the pure material properties listed in Table 1 and an initial ice porosity of 32%, with the pores filled with methane gas at 265 K and 6.2 MPa. The good agreement between the measured and the calculated composite density for porous ice validates our approach of estimating sample density using CT images, and also illustrates the usefulness and power of this technique.
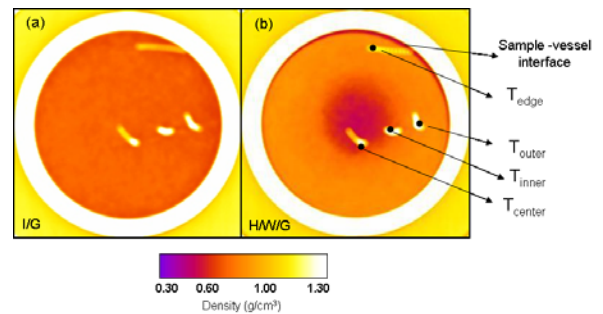

Figure 2.   Average X-ray CT images of 51 (out of 54) cross sections, before (left) and after hydrate formation (right). The outer white circle is the aluminum pressure vessel.

Based on the significant density variation after hydrate formation, the sample was divided into three different zones; the low-density center ($\rho_{avg.}$ = 420

kg/m³; Zone 1), the transition zone (ρ avg. = 545 kg/m³; Zone 2) and the high-density outer zone (ρ avg. = 727 kg/m³; Zone 3). As shown in Equation 2a, the composite density reflects the combined contributions of the hydrate, water and gas phases. Because we have three unknowns in each zone (S_H, S_G, and S_W) and two independent relationships (i.e., Equations 2b and 3), it is not possible to determine the unique phase saturation values of hydrate, water, and gas phases in each zone. Therefore, we obtained the range of phase saturations that satisfies Equations 2b and 3, using the simple iterative procedure, described below.

$$\rho_\theta = \rho_G S_G + \rho_H S_H + \rho_W S_W \qquad (2a)$$

$$\text{where } S_H = \frac{V_H}{V_z} \; ; \; S_G = \frac{V_G}{V_z} \; ; \; S_W = \frac{V_W}{V_z}$$

$$\rho_\theta = \rho_G S_G + \rho_H S_H + \rho_W (1 - S_H - S_G) \qquad (2b)$$

$$S_G + S_H + S_W = 1 \qquad (3)$$

There are only small ranges of S_H, S_G, and S_W values that can satisfy Equations 2b and 3, and also give physically realistic values (i.e., S_H, S_G, and S_W can only take values between 0 and 1). Using the iterative procedure, we calculated between the following $0.562 < S_{G,\ Zone1} < 0.602$, $0.006 < S_{H,\ Zone1} < 0.434$, and $0.004 < S_{W,\ Zone1} < 0.392$ for Zone 1. Applying this procedure to Zones 2 and 3, ranges of S_G, S_H, and S_W were calculated for Zones 2 and 3, using the composite density from the CT images in Zones 2 and 3, respectively.

Finally, to ensure that the mass balance of all phases was satisfied, we determined the combinations of phase saturations of hydrate, water, and gas in each zone. This was performed by minimizing the difference between the corresponding estimated and measured mass of each phase.

After determining the combinations of saturations in Zones 1, 2, and 3, we computed the range of composite-specific heats (C_θ) from:

$$C_\theta = C_W X_W + C_H X_H + C_G X_G \qquad (4)$$

where X is the mass fraction of each phase.

Using values of C_W, C_H, and C_G (Table 1), the composite specific heats of Zones 1 to 3 were determined. The estimated range of specific heat values in each zone was used in the inverse modeling simulations to estimate the sample composite thermal conductivity.
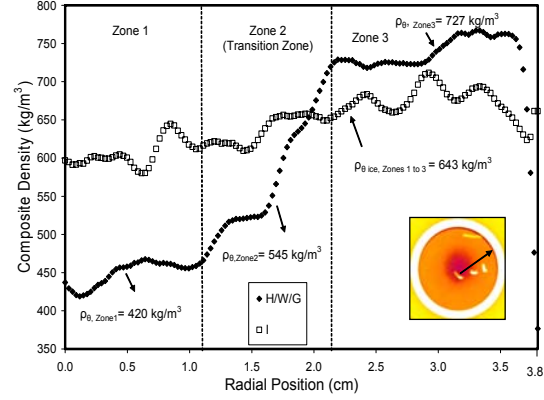

Figure 3. Measured composite density in the radial direction. The porous ice density was averaged along the arrow shown in the CT image. The sample composite density changed in the radial direction after hydrate formation. Based on the density variation, the core was divided into three different regions i.e. Zones 1, 2, and 3.

THERMAL TESTS

The temperature response of the sample was measured over time using the thermocouples denoted as T_{outer}, T_{inner}, and T_{center} in Figure 2. We conducted two thermal tests at pressure and temperature conditions within the methane hydrate stability zone. The equilibrium temperature of methane hydrate is 279.6 K at 4.98 MPa. The first thermal test involved a step-wise decrease of the bath temperature from 279.1 K to 277.3 K at a constant pressure of 4.98 MPa. In the second thermal test, the bath temperature was increased from 277.3 K to 279.1 K at 4.98 MPa. Temperature data were collected every 20 seconds using a Keithley 2750 data acquisition system. In both tests, pressure was also continuously monitored.

Phase	C (J/kg/K)	ρ (kg/m³)	k (W/m/K)
Ice	2040	917	2.23
Hydrate	2080	910	0.575
Water (at 4.98 MPa, 277 K)	4188	1000	0.57
Methane Gas (at 4.98 MPa, 277 K)	2612	38.9	0.035

Table 1. Pure phase properties

COMPOSITE THERMAL CONDUCTIVITY ESTIMATION AND VALIDATION

In this study, we determined the composite thermal conductivity of a porous methane hydrate sample

(consisting of hydrate, water, and gas) by a history-matching technique using iTOUGH2 [*Finsterle*, 1999]. iTOUGH2 is capable of handing nonreactive phases, and in this case hydrate does not pose any problems because both tests were performed under thermodynamically stable hydrate conditions.

The cylindrical hydrate sample was assumed to be axially symmetric and was modeled as a one-dimensional radial system. The domain, consisting of the composite hydrate sample (containing hydrate, water, and methane gas) was divided into 380 gridblocks of uniform $\Delta r = 10^{-4}$ m. Owing to heterogeneity in the radial direction, we divided the hydrate sample into three different zones. The exact length of each zone and location of each thermocouple were determined from the CT images. This information was used to assign the thermal data in the radial direction in the simulations.

In Figure 2b, the CT image shows the presence of a gas gap between the sample and the aluminum vessel wall. This gap width is non-uniform and is expected to result in a non-uniform heat flux between the sample and the bath. To address this problem, we used conditions at the outer thermocouple as the outer boundary (instead of those in the bath) in the simulation.

For the radial heat conduction process, the rate of heat flow is dictated by the medium thermal diffusivity [$(\alpha = k / (\rho*C)$]. Because of nonflowing conditions, we assume no advective flow, and consequently heat transfer occurs only through conduction. We assigned the composite sample density and specific heat to each zone in the simulation. The gridblocks within the same zone had the same value of composite density and specific heat. Subsequently, we estimated the composite thermal conductivity (k_θ) of each zone by minimizing the differences between the observed and predicted thermal response using history matching. The optimal k_θ values in Zones 1 to 3 were determined using the following procedure.

The thermal conductivity estimation process involved two steps. In Step 1, individual zone composite thermal conductivities (k_θ) were optimized and estimated by inverse modeling of the first thermal data set using iTOUGH2 (as described above). In the inverse modeling, we used the conditions at the outer thermocouple as a boundary and predicted the temperature response of the two internal thermocouples.
Figure 4 shows the comparison between observed and predicted temperature versus time profiles during the first thermal test (decreasing the temperature from 279.1 to 277.3 K), for the optimal values of $k_{\theta,Zone\ 1}$, $k_{\theta,Zone\ 2}$, and $k_{\theta,Zone\ 3}$, equal to 0.25, 0.45 and 0.58 W/m/K, respectively.
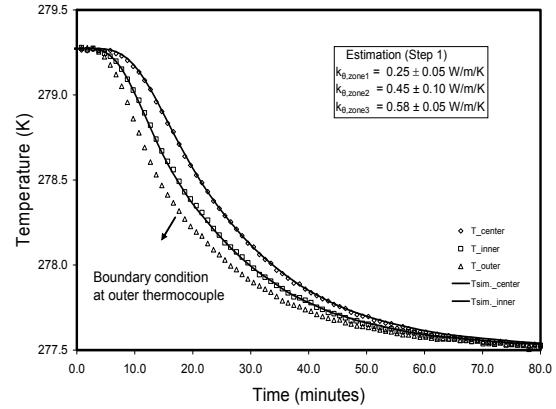

Figure 4. Calibration and parameter determination from cooling data in the H/W/G system by inverse modeling. The symbols represent data, and lines represent model results.

These optimized values of composite thermal conductivity were consistent within ±0.05 W/m/K for Zones 1 and 3 and ±0.10 W/m/K for Zone 2. In contrast to Zones 1 and 3, the composite thermal conductivity of Zone 2 exhibited a relatively larger error in the estimation. The large error in the k_θ estimation in Zone 2 was attributed to the relatively large variation in the bulk density determined from the CT images.

In Step 2, we assigned the estimated composite thermal conductivities (k_θ) to each zone and performed the forward simulation to predict the thermal response at the internal thermocouple locations for the temperature increase at the outer thermocouple (277.3 to 279.1 K). Figure 5 shows the comparison between the observed and predicted temperature versus time profiles for the heating test. The proximity between observed and predicted profiles validated the estimated k_θ for each zone that was derived in Step 1.

The inverse modeling simulations were performed for the entire range of phase saturations determined and yielded the optimal values of composite thermal conductivity (k_θ). For some saturation values, unrealistic saturation values were obtained, e.g., an estimated thermal conductivity in Zone 2 was higher than that in Zone 3, in spite of its lower density. Such cases were omitted from the final results.
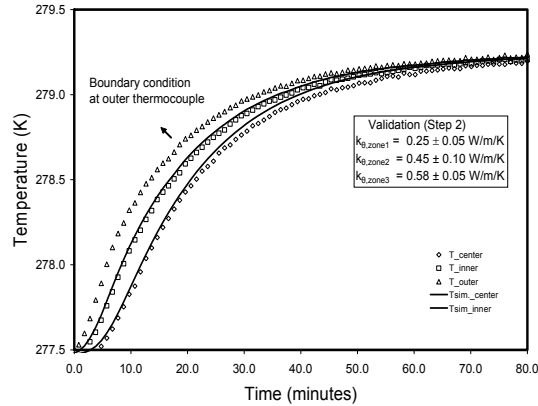
Figure 5. Prediction of heating test response and validation of the parameters ($k_{\theta, zone1}$, $k_{\theta, zone2}$, and $k_{\theta, zone3}$) determined in Step 1. The symbols represent data, and lines represent model results.

CONCLUSIONS

X-ray CT imaging, used to visualize the heterogeneous porous methane hydrate sample, allowed explicit consideration of the sample heterogeneity. CT images showed that the hydrate sample formed from granular ice was heterogeneous, and the composite density increased from 420 kg/m^3 to 727 kg/m^3 from the center to the edge of the sample core.

We used an inverse-modeling technique to estimate the composite thermal conductivity of the porous hydrate sample as a function of density. The estimated k_θ ranged from 0.25–0.58 W/m/K. In the present work, we have shown that the methane hydrate sample formed from granular ice was not homogeneous, and this variation in the sample should be accounted for in the hydrate physical and thermal property measurements. Overall, the present work provides a new technique by which to estimate the thermal conductivity of a porous methane hydrate sample as a function of density using iTOUGH2. This work also demonstrates the importance of x-ray computed tomography in hydrate physical and thermal property measurements.

ACKNOWLEDGMENTS

REFERENCES

Abramoff, M.D., P.J. Magelhaes, and S.J. Ram, Image processing with ImageJ, *Biophotonics International*, *11* (7), 36-42, 2004.

Finsterle, S., iTOUGH2 user's guide, Version 3.1, LBNL-40041, Lawrence Berkeley National Laboratory, Berkeley, 1999.

Kneafsey, T.J., L. Tomutsa, G.J. Moridis, Y. Seol, B.M. Freifeld, C.E. Taylor, and A. Gupta, Methane hydrate formation and dissociation in a partially saturated sand-measurements and observations, *Fifth International Conference on Gas Hydrates, Trondheim, Norway, 1033*, 213-220, 2005.

Milkov, A.V., Global estimates of hydrate-bound gas in marine sediments: How much is really out there?, *Earth Science Reviews*, *66*, 183-197, 2004.

Peters, D., S. Selim, and E. Sloan, Hydrate dissociation in pipelines by two-sided depressurization, experiment and model, *Challenges for the future/gas hydrates, NYAS 912*, 304, 2000.

Ruppel, C., Thermal state of the gas hydrate reservoir, *natural gas hydrate in oceanic and permafrost environments, Max Ed., Book*, 29-42, 2000.

Sloan, E.D., Jr., *Clathrate Hydrates of Natural Gases, Second Edition*, 754 pp. pp., Marcel Dekker, NY, 1998.

Stern, L.A., S.H. Kirby, and W.B. Durham, Peculiarities of methane clathrate hydrate formation and solid-state deformation, including possible superheating of water ice, *Science*, *273*, 1843, 1996.